JOURNAL OF CATALYSIS 111, 383–396 (1988)

Model Studies of the SMSI Phenomenon

I. CO and Hydrogen Chemistry at the Ru–Ti Interface

JAS PAL S. BADYAL, ANDREW J. GELLMAN,[1] AND RICHARD M. LAMBERT[2]

Department of Physical Chemistry, University of Cambridge, Cambridge CB2 1EP, United Kingdom

Received December 6, 1987

Ti films grow on Ru(0001) in a layer-by-layer mode, a $(\sqrt{91} \times \sqrt{91})$R5.2° LEED pattern appearing at loadings close to monolayer completion. Such films are extremely active towards H_2 and CO chemisorption, although in both cases no aggregation of the Ti deposit occurs as a result. The uptake of β-CO (characteristic of clean Ru) is strongly suppressed by Ti dosing: this effect is markedly nonlinear and the results suggest that islands of Ti exert a significant long-range influence on the chemisorption of CO by Ru. Isotope data show that the presence of Ti leads to the formation of dissociatively adsorbed CO, while hydrogen chemisorption results in a surface hydride species of limiting stoichiometry TiH_3. This latter species decomposes at ~600 K with concomitant formation of an Ru–Ti surface alloy; the TiH_3 surface hydride is itself very active in the dissociative chemisorption of CO. The relevance of these findings to aspects of the SMSI phenomenon and to K-promoted Ru is discussed.

INTRODUCTION

Since the initial observations of Tauster *et al.* (*1*), the phenomenon of strong metal–support interaction (SMSI) has attracted considerable interest and speculation. In addition to many classical catalytic studies on metal/reducible oxide systems, there have been several attempts to model certain aspects of SMSI behaviour with the aid of metal foils and single crystals (*2–5*).

The present paper is the first in a series of articles describing the results of a correlated programme involving measurements on both single-crystal TiO_x/Ru systems and Ru/TiO_2, $TiO_x/Ru/SiO_2$, and Ru/SiO_2 high-area catalysts. We report here on the interaction between metallic titanium and a well-characterized Ru(0001) surface; the behaviour of this bimetallic system towards H_2 and CO at low pressures is also described. The formation and decomposition of adsorbate phases and surface compounds are investigated, and these observations lay the foundation for a detailed examination of CO + H_2 chemistry and catalysis at the interface between Ru and TiO_x to be described elsewhere (*6*).

EXPERIMENTAL

Experiments were carried out in an ultra-high vacuum chamber of conventional design which was capable of routinely achieving base pressures of $<2 \times 10^{-11}$ Torr. The system included a multiplexed mass spectrometer for thermal programmed desorption (TPD) measurements and a three-grid retarding field analyser for LEED/Auger measurements. The mass spectrometer ioniser was enclosed in a shield which effectively discriminated against the scattered gas signal from the rear face of the specimen. The resulting TPD signals were therefore dominated by the line-of-sight flux from the crystal front face, and effects due to finite pumping speed were thereby

[1] Permanent address: School of Chemical Sciences, University of Illinois, 505 S. Mathews Avenue, Urbana, IL 61801.

[2] To whom correspondence should be addressed.

0021-9517/88 $3.00

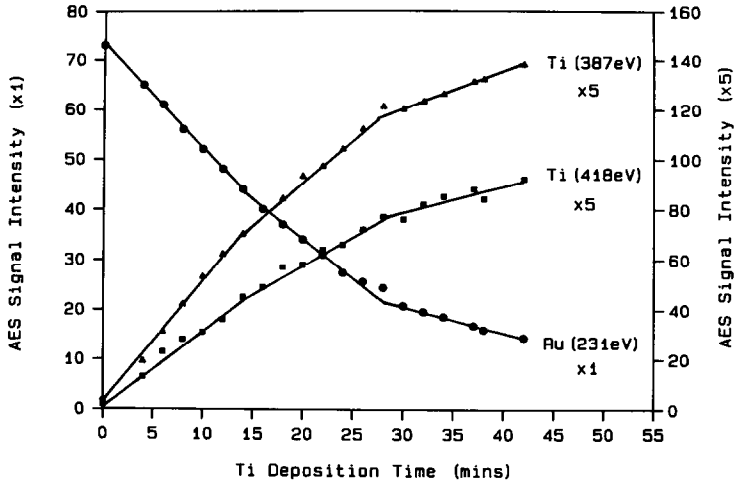

FIG. 1. Ru and Ti AES data as a function of deposition time at 300 K. (The small positive intercept exhibited by the Ti data is due to an underlying weak Ru Auger transition—see text.)

also minimised. In the results which follow, all data therefore refer essentially to Ti deposition on and gas desorption from the front face of the specimen. Sample dosing was carried out using a capillary array gas doser and a collimated resistively heated evaporation source for titanium dosing.

The Ru(0001) specimen was prepared from a 99.99+% pure ingot by standard methods and also mounted onto a sample holder which could be cooled to 140 K and resistively heated using a programmable heating supply. Cleaning was achieved (*7*) by heating to 1350 K in 10^{-7} Torr oxygen, followed by flashing to 1550 K under ultrahigh vacuum to remove traces of subsurface oxygen (*8*). Extreme care was taken to ensure that in all experiments the sample was free from dissolved titanium; this was achieved by leaching out bulk Ti using repeated cycles of heating in oxygen (1250 K/10^{-7} Torr) and Ar^+ etching until the Auger spectrum characteristic of clean ruthenium was obtained (*9*). In this connection, we have already reported in detail (*9*) on the assignment of certain significant features which appear in the Auger spectrum of Ru(0001). As explained in Ref. (*9*), these features may be variously assigned to Ru Auger transitions, diffraction features, or the presence of impurity Ti. The Auger and diffraction features were identified and it was shown that signals from impurity Ti were undetectable with a rigorously cleaned specimen. All gas exposures were corrected for ion gauge sensitivities (*10*).

RESULTS AND ANALYSIS

Deposition of Titanium onto Ru(0001)

Deposition of ultrathin titanium films proved to be sensitive to background impurities, so great care was taken to ensure that the titanium source was fully outgassed before each experiment, a chamber pressure of 1×10^{-10} Torr being maintained throughout the deposition stage. Figure 1 shows the variation of titanium and ruthenium Auger signals as a function of deposition time at 295 K, deposition being shown to be uniform across the crystal to within 5%. Breaks are apparent in the uptake curves at regular deposition intervals in both the ruthenium and the titanium AES data; this is characteristic of monolayer-by-monolayer growth (Frank–van der Merwe growth (*11*)). The ratio of the intensities of the Ti (387-eV) AES signal to the Ru (231-eV) AES signal can be taken to be characteristic

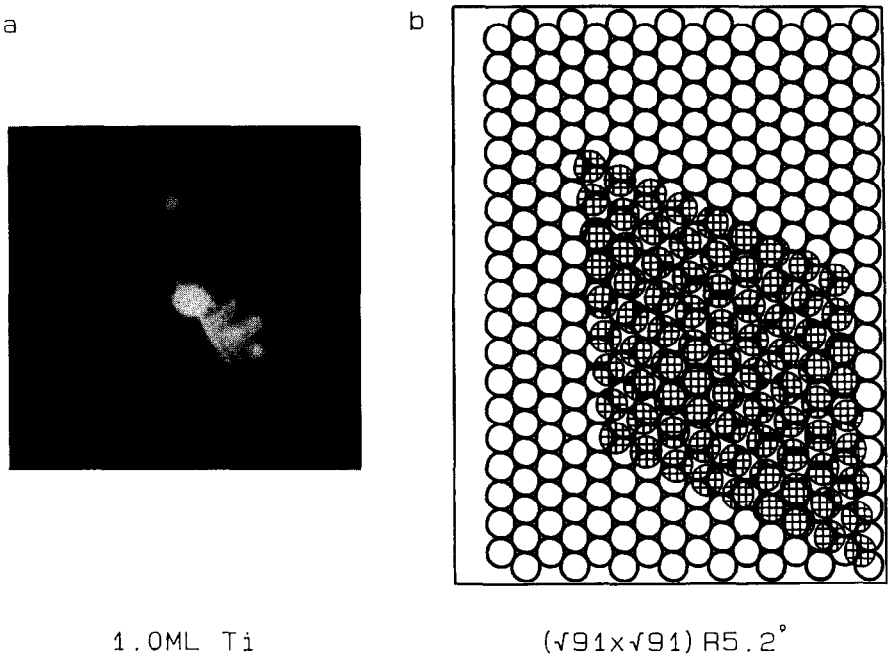

FIG. 2. (a) ($\sqrt{91} \times \sqrt{91}$)R5.2° LEED structure observed in the region of monolayer completion; beam energy 48.8 eV. (b) Proposed Ti overlayer structure for the $\sqrt{91}$ phase.

of the breakpoints: the first breakpoint corresponds to a signal ratio of 0.31 ± 0.03 and the second breakpoint corresponds to 0.91 ± 0.15.

The clean ruthenium surface gave a bright and fairly sharp (1 × 1) LEED pattern which underwent a marked increase in background intensity during the early stages of Ti deposition at 300 K. No new LEED patterns were obtained at this point, indicating that titanium atoms were randomly distributed over the ruthenium surface, or that small titanium aggregates, the size of which was less than the coherence width of the electron beam, were present. In the region of monolayer coverage, a weak LEED pattern appeared and sharpened up slightly on annealing to 420 K (Fig. 2a). This LEED pattern may be interpreted in terms of the coincidence lattice structure illustrated in Fig. 2b, a view which is at least consistent with the growth mode indicated by the Auger data: i.e., this structure appears at a Ti loading corresponding to the first break point in the Auger data. The ideal structure may be indexed as a ($\sqrt{91} \times \sqrt{91}$)R5.2° hexagonal phase in which the Ti–Ti separation is 3.138 Å (cf. 2.896 Å in bulk hcp titanium (*12*)).

CO Chemisorption

Characteristic CO thermal desorption spectra from the clean Ru(0001) surface following chemisorption at 300 K are shown in Fig. 3. The high-temperature desorption peak saturates at a coverage which corresponds to the intensity maximum of a ($\sqrt{3} \times \sqrt{3}$)R30° LEED pattern (θ_{CO} = 0.33 monolayer), thus providing an absolute coverage calibration for both CO and hydrogen uptake measurements (*13, 14*), due allowance being made for relative mass spectrometer sensitivities. A second peak appears at higher CO coverages and has been ascribed to the effect of repulsive interactions within the adsorption layer (*13*). The surface saturated after an exposure of 44 L CO (1 L = 10^{-6} Torr sec) in close

agreement with values obtained by other workers (*13, 15*). Angle-resolved UPS (*16*), IRAS (*17*), HREELS (*18*), NEXAFS (*19*), and ESDIAD (*20*) studies coherently illustrate that CO is terminally bonded at the Ru surface, high coverages being accommodated by continuous tilting of the linearly coordinated molecules.

CO adsorption on Ti-dosed Ru leads to the appearance of two new features in the desorption spectra, in addition to the clean surface β peaks. These comprise a high-temperature peak (~1000 K) which shifts to higher temperatures with increased Ti loading, and a low-temperature peak (~180 K) which could not be examined in quantitative detail because of limitations of the specimen cooling system ($T_{min} \sim 140$ K). Experiments were carried out with isotopically labelled CO in order to clarify the nature of these new binding states; 1 : 1 mixtures of $^{13}C^{16}O$ and $^{12}C^{18}O$ were adsorbed, after which the following species were monitored simultaneously in a subsequent desorption experiment.

Atomic mass	Species detected
28	($^{12}C^{16}O$)
29	($^{13}C^{16}O$)
30	($^{12}C^{18}O$)
31	($^{13}C^{18}O$)
44	($^{12}C^{16}O_2$)
45	($^{13}C^{16}O_2$)
46	($^{12}C^{16}O^{18}O$)

Typical results are illustrated in Figs. 4A–4D which clearly reveal the nature of the three different CO species. As expected, the β "clean surface" molecular CO peak does not exhibit the effects of isotope scrambling (Fig. 4A); the same is true of the low-temperature α feature (Fig. 4D). However, the high-temperature γ peak clearly shows the effects of scrambling (Figs. 4B and 4C) indicating dissociative adsorption of the corresponding CO species. Note that CO_2 desorption was never detectable (mass 44 trace). All the data acquired at 28, 29, 45, and 46 amu were entirely consistent with

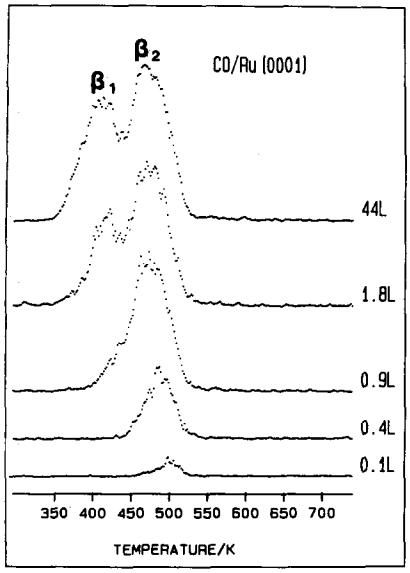

FIG. 3. β-CO desorption from clean Ru(0001) following chemisorption at 300 K. Heating rate 11 K/sec.

the 30, 31, and 44 amu results shown in Fig. 4. Taken together, these results strongly suggest that the new desorption features are associated with Ti sites. It was found that desorption sweeps of the Ru/Ti/CO system to temperatures in excess of ~800 K led to some diffusion of carbon into the bulk of the metal. This is the temperature regime in which Ru–Ti alloy formation commences (*6*) so it seems plausible that under these conditions incorporation of adsorbate atoms into the metal could occur. For this reason, no further investigation of the high-temperature CO desorption feature was carried out.

The dependence of the β-CO peak on Ti loading can be used to probe the environment of Ru atoms in the vicinity of the Ti deposit. Figure 5A shows that following a saturation dose of gas, the CO desorption features characteristic of clean Ru(0001) are uniformly suppressed with increasing titanium coverage, no change in peak temperature or peak shape being observed. Since the diffusion of titanium or titanium compounds into the bulk has been shown to be insignificant at temperatures associated

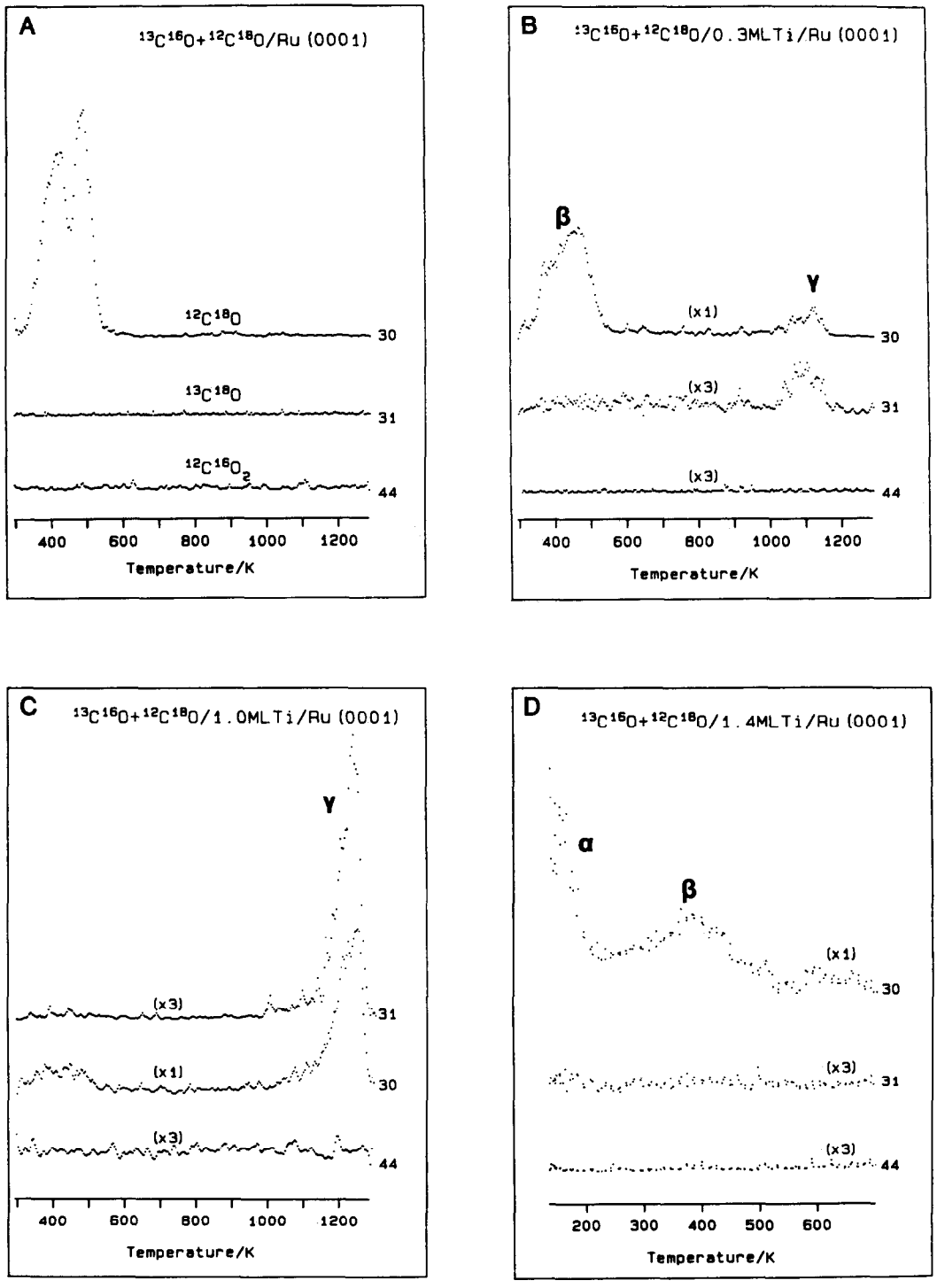

FIG. 4. CO chemisorption on Ti-dosed Ru. Use of isotopes to examine α, β, and γ states. (A) Clean Ru(0001); (B,C) with Ti predoses of 0.3 and 1.0 monolayer, respectively. (D) Shows low-temperature α peak at 1.4 monolayers Ti precoverage.

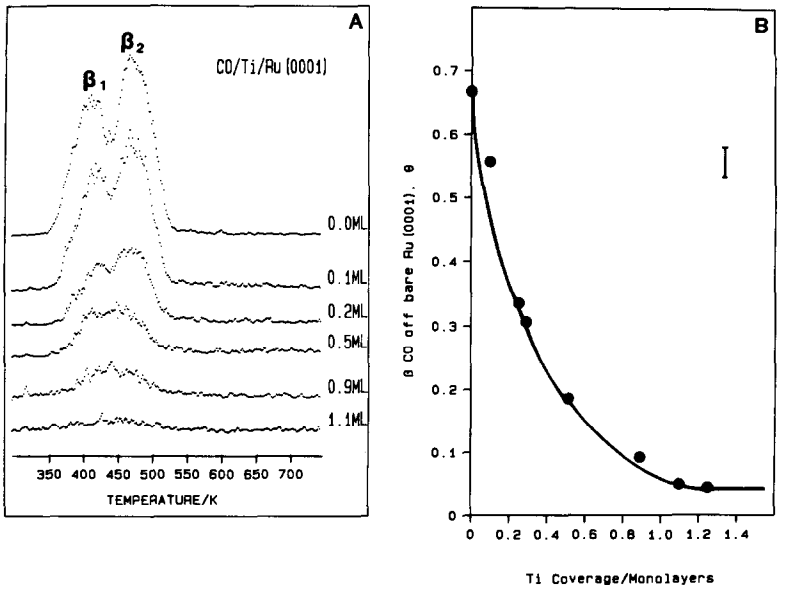

FIG. 5. Effect of Ti predosing on uptake of β-CO by Ru. (A) β-Desorption spectra as a function of Ti precoverage. (B) β-Desorption yield as a function of Ti coverage.

with CO desorption from clean Ru(0001) (*6*), all the chemistry can be considered to occur in two dimensions during the desorption of molecular CO from bare ruthenium sites. Figure 5B is a plot of the integrated CO desorption yields. It is apparent that the chemisorptive capacity of the Ru surface is a nonlinear function of the Ti coverage, possible explanations for which could include the following:

(i) a Ti/C/O compound forms which "spreads" on the Ru surface,

(ii) CO chemisorption on Ru requires a critical ensemble of Ru atoms,

(iii) Ru sites around the edges of the Ti deposits are electronically modified so that β-CO chemisorption is suppressed.

We now examine each of these possibilities in turn.

The first seems unlikely, since it would be expected to lead to complete suppression of the unimpaired ruthenium sites at titanium coverages well below a monolayer.

If ensemble effects operate and Ti atoms are distributed randomly on the underlying Ru, it can be shown (*21*) that

$$\theta_{CO} \propto (1 - \theta_{Ti})^n,$$

where n is the number of active Ru atoms required to adsorb one CO molecule. Likewise, the number of CO molecules prevented from adsorbing is given by (*22*)

$$(1 - (\theta_{CO}/\theta_{CO(sat)})) \propto \theta_{Ti}^n.$$

Bilogarithmic plots of both these equations should therefore yield straight lines if blocking of β-CO is the result of Ru ensemble effects arising from a random distribution of Ti adatoms: Figures 6A and 6B demonstrate that this is not the case.

Finally, if the Ti deposit evolves in the submonolayer regime by a nucleation and growth mechanism in which a constant number of circular two-dimensional islands grow at a uniform rate, then it may be shown that

$$(1 - (\theta_{CO}/\theta_{CO(sat)}^{1/2})) = \theta_{Ti}^{1/2} + \pi^{1/2} n_s^{1/2} \delta r,$$

where n_s is the number density of nucleation sites and r measures the distance

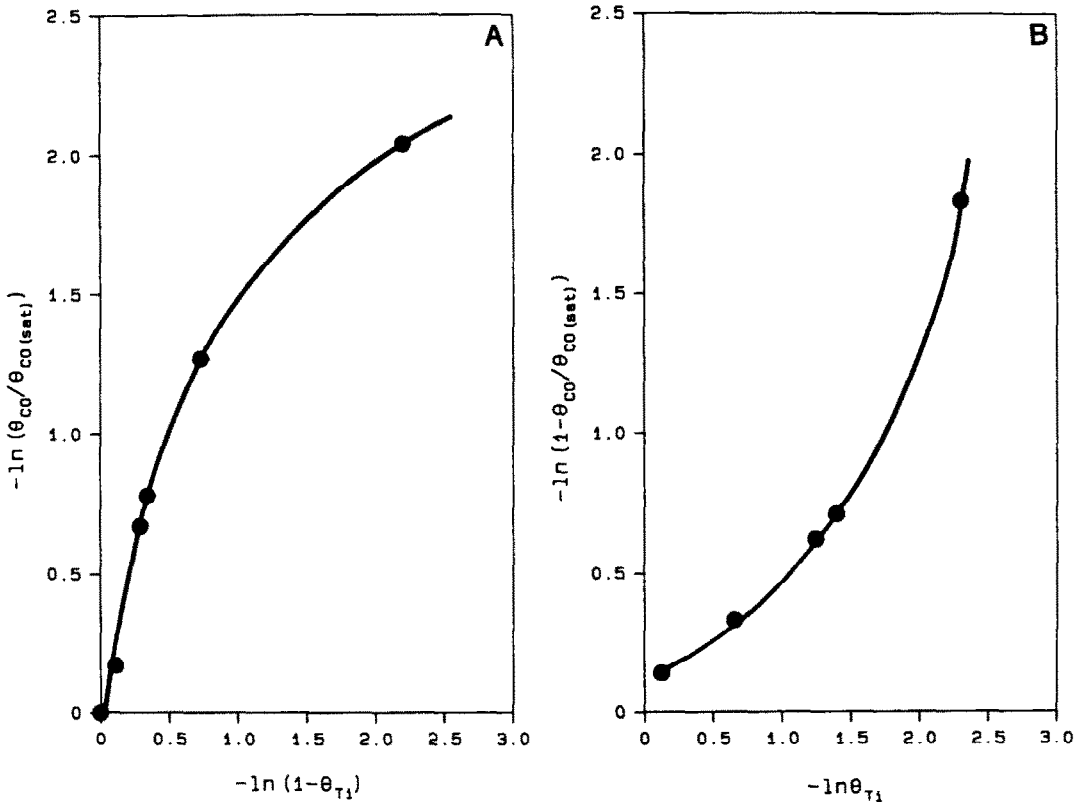

FIG. 6. Ti blocking of β-CO; tests of simple ensemble model.

over which β-CO suppression is induced. Figure 7 shows a plot of the data in terms of this equation; reasonable agreement up to a Ti precoverage of ~0.3 monolayer is found. At higher Ti loadings the amount of β-CO blocking observed is less than predicted. In terms of this simple model, the most likely explanation for the deviation is that overlap of island perimeters eventually occurs at sufficiently high Ti loadings; the data do in fact permit an estimate of $n_s^{1/2}\delta r$ to be made, but δr itself cannot be evaluated since we have no independent measure of n_s.

H_2 Chemisorption

Thermal desorption data following H_2 adsorption on clean Ru(0001) at 140 K are in accord with earlier work (*23–25*). A single peak (β_2) appears at low coverage, followed by a poorly resolved low-temperature feature (β_1) at high coverages (Fig. 8). Ti predosing leads to two interesting effects on the subsequent uptake of hydrogen (Fig. 9A) for gas exposures close to the saturation value (200 L). At low Ti coverages there appears to be an increase in β_1-hydrogen. This effect is maximised at about 0.3 monolayer Ti coverage, beyond which point the β_1, β_2 states are progressively suppressed (Figs. 9A and 9B). The other important aspect of Fig. 9A is the appearance of a sharp desorption feature (γ) at high temperature; this first appears in the submonolayer regime, increasing in intensity and shifting to higher temperatures with increasing Ti loading.

The results illustrated in Fig. 9A were obtained by rigorously cleaning the surface (Ar^+ etching) before depositing a fresh loading of Ti prior to each experiment. Examination of the surface by LEED after a desorption sweep revealed the presence of

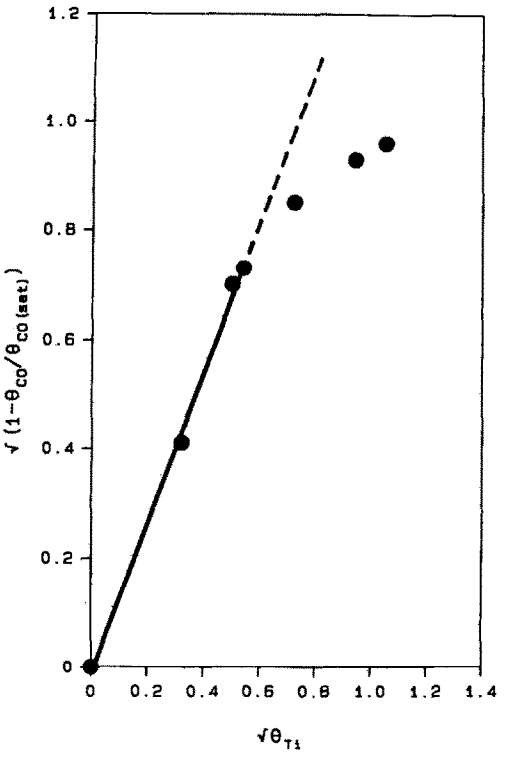

FIG. 7. Ti blocking of β-CO; test of Ti island model.

structures characteristic of Ti–Ru surface alloys (*6*). It is also noteworthy that the γ-H_2 peak appears in a temperature regime where Ti–Ru surface alloys are formed from Ti overlayers on Ru(0001) (*6*). It seems likely therefore that γ-H_2 evolution is accompanied by surface alloy formation; a subsequent exposure of this alloy surface to more hydrogen did not result in repopulation of the γ state (Fig. 9C). Closer examination of the data shows that the temperature of the γ-H_2 peak tends to a limiting value in the region of monolayer Ti coverage (Fig. 10A). This observation and the almost complete disappearance of the β peaks at ~1 monolayer Ti indicate that, as with CO, hydrogen chemisorption does not lead to aggregation of the Ti film with concomitant exposure of bare Ru sites. Assuming that the γ-hydrogen is associated with Ti, it is possible to calculate the Ti : H stoichiometry of the surface phase as a function of Ti loading (Fig. 10B). It can be seen that this quantity changes rapidly in the vicinity of Ti monolayer completion, eventually approaching a value which suggests the formation of a phase TiH_3, followed by a decline towards the stoichiometry of the bulk hydride (TiH_2). An estimate of the activation energy for H_2 desorption from the Ti/H phase can be obtained from Arrhenius plots of the desorption data; these indicate values ranging from 100 ± 40 kJ/mol at 0.5 monolayer Ti to 195 ± 40 kJ/mol at 1.5 monolayers Ti. The enthalpy of decomposition of bulk TiH_2 is 120 kJ/mol (*12*).

CO/H_2 Interaction on Ti/Ru(0001)

It is known that CO dosing of a clean Ru(0001) surface precovered with chemisorbed hydrogen does not lead to any displacement of the latter and results only in a slight perturbation of the hydrogen binding energy (*26*). This observation is confirmed by our own measurements. However, the situation is completely altered in the pres-

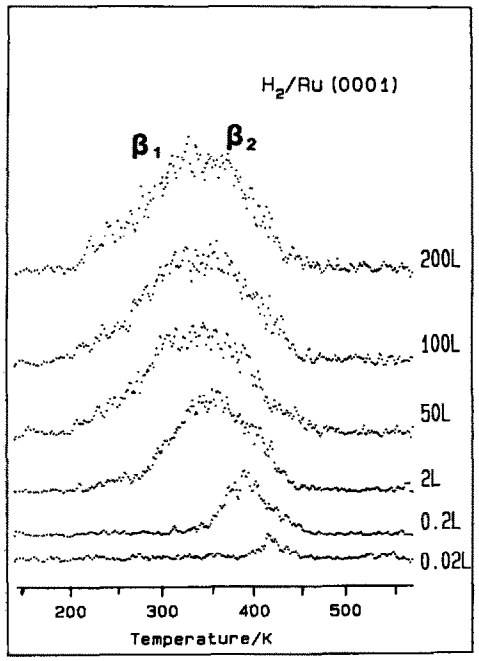

FIG. 8. Hydrogen desorption from clean Ru(0001) following chemisorption at 140 K.

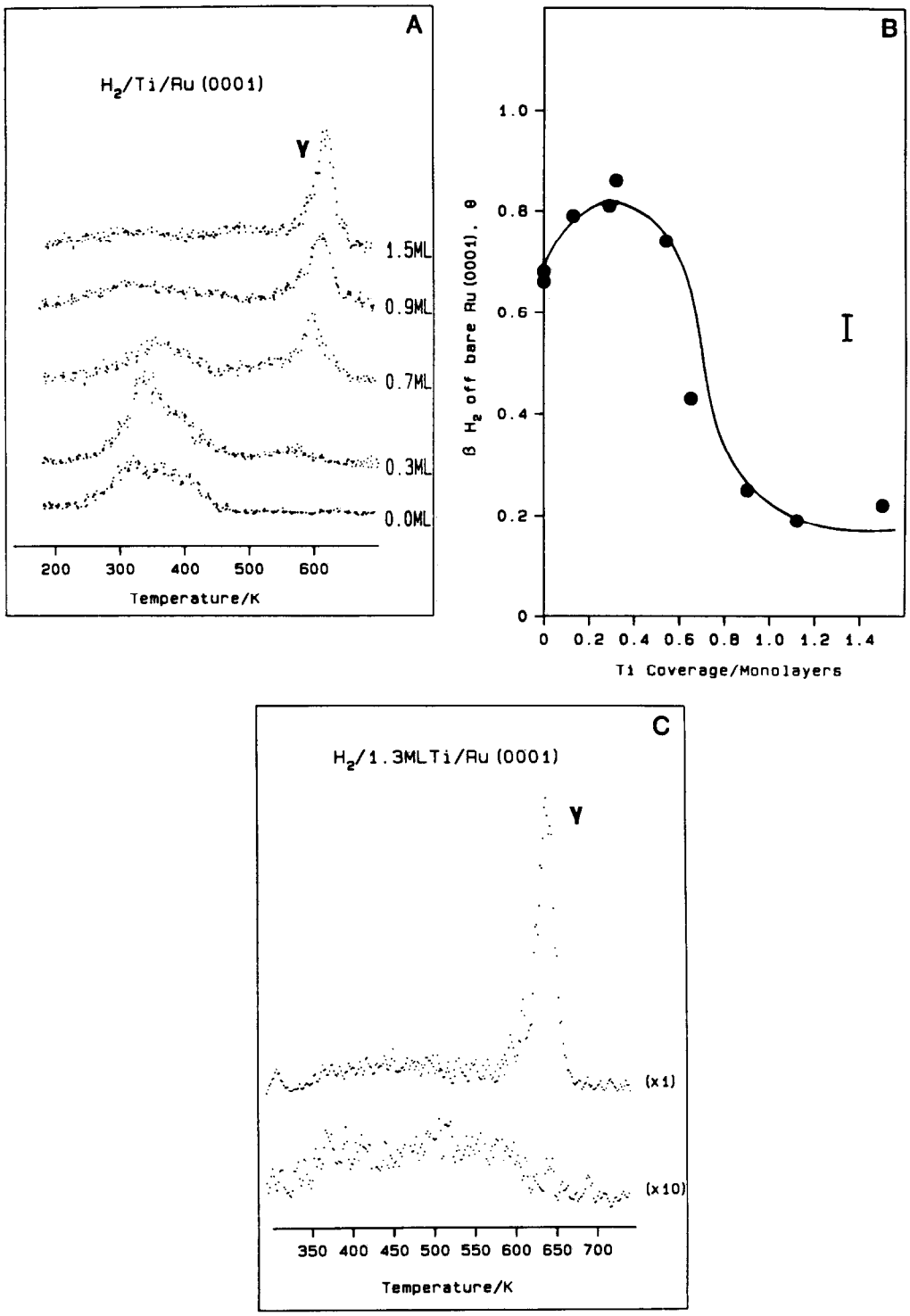

FIG. 9. Effect of Ti on subsequent uptake and desorption of hydrogen, showing effect of β and γ states. (A) Desorption spectra as a function of Ti coverage. (B) β-H_2 yields as a function of Ti coverage. (C) Shows hydrogen uptake characteristics of fresh Ti overlayer and of Ti–Ru surface alloy formed after decomposition of γ-phase.

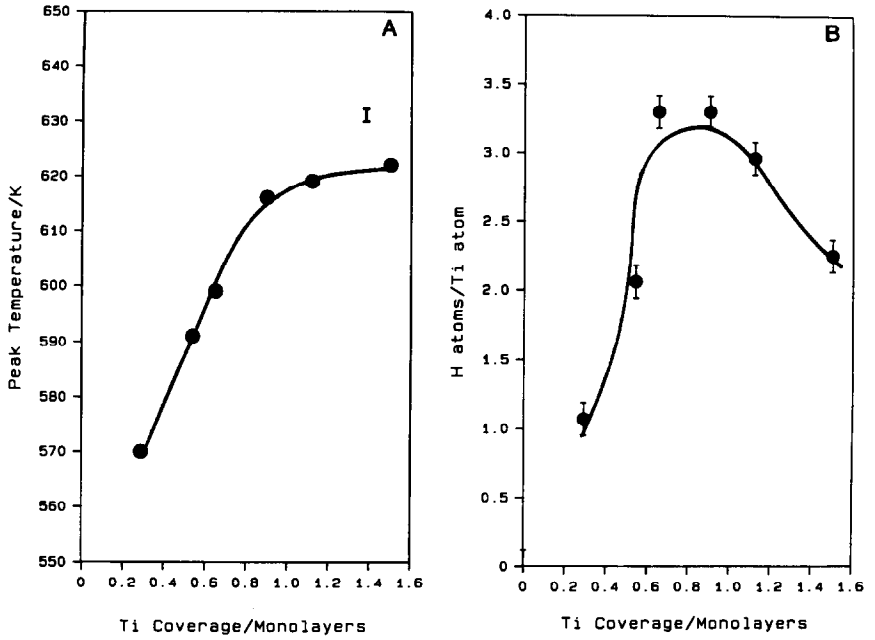

FIG. 10. (A) Dependence of γ-H_2 peak temperature on Ti precoverage. (B) Dependence of hydride phase stoichiometry on Ti loading.

ence of Ti. Thus during and after an exposure of 44 L of CO to a TiH_x ($x \sim 3$) film (prepared as described above) a large destabilisation of the hydrogen associated with Ti occurs. Very little CO desorption takes place from such a surface (Fig. 11) and no desorption products were detectable at 16, 18, 27, 30, or 32 amu. At the same time, carbon and oxygen characteristic of dissociated CO could be seen in the Auger spectrum after the desorption sweep. It thus appears that the TiH_x film is very active for CO dissociation, a process which also leads to very pronounced destabilisation of the γ-hydrogen initially present in the surface layer.

DISCUSSION

Titanium Deposition on the Ru(0001) Surface

The layer-by-layer growth mode found here for Ti on Ru(0001) is a common observation in many metal-on-metal systems. It indicates that the Ti–Ru interaction is stronger than the Ti–Ti interaction, which is at least consistent with the relative sublimation energies of the two pure metals. The proposed ordered overlayer phase which forms in the vicinity of monolayer completion is very similar to that proposed for Li overlayers on Ru(0001), a system which gives rise to essentially the same LEED pattern (*27*). In the present case, the structure illustrated in Fig. 2b corresponds to a Ti–Ti spacing which is ~8% greater than the corresponding distance in pure hcp Ti.

CO/Ti/Ru(001)

Bonding of transition metals to CO is frequently discussed in terms of Blyholder's model (*28*), and the ability of Ru surfaces to dissociate CO has been related to the degree of electron back-donation to the CO 2π orbital. In some aspects, the CO/Ti/Ru(0001) model system appears to be similar to the extensively investigated CO/K/Ru(0001) system. In the latter case it has been shown that for high exposures of CO to submonolayer potassium coverages there exist two CO adsorption sites, one in

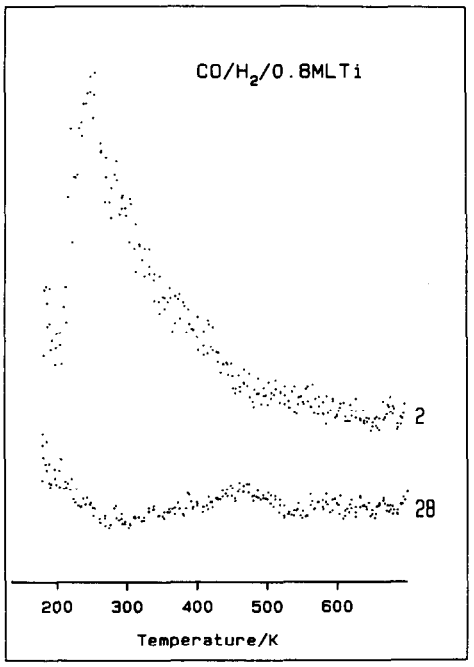

FIG. 11. CO chemisorption on surface hydride showing suppression of molecular states and drastic destabilisation of γ-H_2.

the vicinity of potassium atoms, the other associated with CO on areas further removed from potassium (referred to as "bare" Ru(0001)) (*29*). CO molecules in the vicinity of an alkali atom receive "through-metal" charge transfer from the adsorbed potassium (*30*); this is believed to lead to either rehybridisation of the Ru–CO bond to sp^2 (*31*) or electron donation into antibonding molecular orbitals of CO (*32*); in both cases the result is intramolecular bond weakening and an increase in adsorption energy.

Our isotope data strongly suggest that the α and β CO states are associative whereas the γ state consists of adsorbed C and O atoms. It is envisaged that growing islands of Ti lead to the chemisorption on Ru of progressively larger amounts of strongly bound (dissociated) γ-CO in the vicinity of the island boundaries. This occurs at the expense of β-CO chemisorption, and the nonlinear dependence of this quantity on Ti coverage suggests that the electronic influence of Ti extends significantly beyond the island boundaries. Given the ability of bulk Ti to dissociate CO (*33*) it seems likely that CO also adsorbs dissociatively on the Ti deposit islands themselves. Subsequent heating leads to the recombination of C and O atoms on and near the Ti resulting in the high-temperature, narrow γ-CO peak.

The shape of the γ-CO peak is reminiscent of that seen for the CO/K/Ru(0001) system (*34*) where an autocatalytic decomposition is thought to occur. The CO/Ti/Ru system is, however, further complicated by the known (*6*) rapid surface to bulk diffusion of Ti which occurs in this temperature regime. One possible explanation, therefore, is that CO is released into the gas phase from in and around the Ti islands as Ti diffuses away into the underlying Ru. It is possible that this process might be "autocatalytic" if the C and O atoms actually inhibit Ti diffusion. However, it is also apparent that the γ-CO peak exhibits features characteristic of fractional order desorption kinetics. This could result from a situation in which γ-CO desorption takes place from Ru at the edges of Ti islands, C + O atoms being supplied by diffusion from the Ti; according to this model, however, the desorption peak should be attenuated completely for Ti precoverages greater than 1 monolayer, whereas Figs. 4B and 4C show that the γ desorption feature increases with titanium loading. This explanation therefore appears to be untenable, and we favour the possibility first put forward. The weakly bound α state which appears at Ti loadings greater than one monolayer is presumably associated with adsorption on Ti. (Control experiments established that this feature was not due to the support wires.)

H_2/Ti/Ru(0001)

The small but genuine Ti-induced increase in the uptake of β-hydrogen at low Ti coverages may be due to the operation of a spillover effect. As stated above, near-saturation exposures of H_2 were used such

that the coverage of bare Ru sites was close to its maximum value. The presence of a relatively low coverage of Ti which assists H_2 dissociation could enhance the surface population of hydrogen under these adsorption rate limited conditions.

The γ-hydrogen peak can be accounted for in terms somewhat similar to the explanation put forward for the γ-CO peak; in this case the apparent fractional order behaviour is more pronounced. All the observations can be rationalised in terms of the formation and destruction of a titanium hydride surface compound. As monolayer coverage is approached (i.e., with decreasing Ti dispersion) an essentially continuous titanium hydride film of nominal stoichiometry TiH_3 is formed. The normal bulk hydride has stoichiometry TiH_2, suggesting that in this case some of the H atoms lie between the Ti overlayer and the Ru beneath. This would be consistent with the structure of the bulk hydride; as for sufficiently thick Ti films the stoichiometry should then approach TiH_2. (Again, we have a parallel with the K/Ru system which has recently been shown to form a surface hydride species (*35*).) γ-H_2 desorption is then the result of the decomposition of this compound accompanied by Ti–Ru alloy formation. Not only has such alloy formation been demonstrated in this temperature regime but also the results in Fig. 9C show that after γ-hydrogen desorption the (alloy) surface no longer chemisorbs γ-hydrogen. The characteristic coverage dependence of the γ-hydrogen peak temperature may reflect a variation in desorption activation energy due to the increasing size of hydride aggregates and/or the observed change in Ti/H stoichiometry.

$CO/H_2/Ti/Ru(0001)$

Some of the present findings are of interest with respect to the SMSI phenomenon, especially on TiO_2-supported catalysts. Two of the more important ideas which have been put forward to account for SMSI behaviour are (a) the formation of an intermetallic compound between reduced Ti and the transition metal component (*1*) and (b) the concept of hydrogen spillover to form species such as $(Ti–H)^{3+}$ (*36*). We have shown that ultrathin films of TiH_x on Ru are capable of dissociating CO very efficiently without undergoing any loss of hydrogen. Such a species, generated from Ru/TiO_2 during high-temperature reduction by the sequence

$$Ru/TiO_2 \rightarrow \text{RuTi intermetallic} \rightarrow RuTiH_x$$

could be responsible for changes in catalytic behaviour. One possible catalytic cycle is shown in Scheme 1. The formation of $Ru–Ti–H_x$ from an Ru–Ti intermetallic phase under strongly reducing conditions seems plausible in view of (a) the thermal stability found here for the $Ru–Ti–H_x$ phase under vacuum and (b) the known tendency of some intermetallic compounds between transition metals and electropositive metals to undergo phase separation into the transition metal and the hydride of the electropositive metal under reducing conditions (*37*).

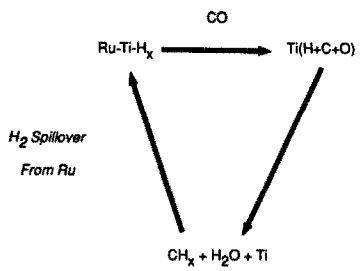

SCHEME 1

Finally, it is of interest to consider the similarities in behaviour towards CO and H_2 found here for Ti on Ru and the behaviour of K-promoted Ru. These resemblances appear even more striking when one considers the characteristic changes in Fischer–Tropsch activity exhibited by Ru/TiO_2 under the SMSI condition (*38*, *39*) and the behaviour of alkali-promoted Ru in the same reaction (*40*). In both cases there is a shift to higher-molecular-weight products

and an increase in the olefin/paraffin ratio. It has also been recently reported (*41*) that such alkali promoters inhibit CO and H_2 chemisorption on Ru/SiO_2 in a manner similar to that of the SMSI effect. Taken together, these observations tend to suggest that alkali promotion and the SMSI effect involve closely related phenomena. Interestingly enough, potassium and TiO_2 exhibit a marked synergism as promoters on Ru; K-doped Ru/TiO_2 catalysts exhibit SMSI behaviour *even after only low-temperature reduction* (*42*), and the Pt/TiO_2 system is known to behave in a similar manner (*43*).

CONCLUSIONS

1. LEED, Auger, CO uptake, and TiH_x stoichiometry measurements are consistent with the view that Ti grows on Ru(0001) in a layer-by-layer mode. Exposure of the Ti film to CO and H_2 leads to strong chemisorption and (in the latter case) the formation of a definite surface compound. In neither case does the interaction lead to agglomeration of the Ti deposit with concomitant exposure of Ru sites.

2. The nonlinear dependence of β-CO uptake on Ti loading suggests the existence of significant long-range effects of Ti on Ru sites; at the same time, isotope data indicate the formation of a Ti-induced, dissociatively chemisorbed CO state.

3. Hydrogen uptake leads to the formation of a surface titanium hydride whose stoichiometry is close to TiH_3 for metal loadings approaching a monolayer; beyond this, the stoichiometry tends towards that of the bulk hydride (TiH_2).

4. This surface titanium hydride decomposes to release hydrogen accompanied by the formation of a Ru–Ti surface alloy. Furthermore, the surface hydride is itself very active in the dissociative chemisorption of CO.

5. There appear to be significant similarities between the Ru–Ti system and the Ru–K system in their behaviour towards CO and H_2. These findings, along with the similarities in catalytic performance between K-promoted Ru and Ru catalysts in the SMSI state, suggest that there may be a close relationship between the two systems.

ACKNOWLEDGMENTS

J.P.S.B. acknowledges financial support by the Science and Engineering Research Council and BP Research Company Plc under CASE Studentship No. CB020. We are grateful to Johnson Matthey Ltd. for a loan of precious metals.

REFERENCES

1. Tauster, S. J., Fung, S. C., and Garten, R. L., *J. Amer. Chem. Soc.* **100,** 170 (1978).
2. Chung, Y. W., Xiong, G., and Kao, C. C., *J. Catal.* **85,** 237 (1984).
3. Demmin, R. A., Ko, C. S., and Gorte, R. J., *J. Phys. Chem.* **89,** 1151 (1985).
4. Dwyer, D. J., Cameron, S. D., and Gland, J., *Surf. Sci.* **159,** 430 (1985).
5. Levin, M. E., Salmeron, M., Bell, A. T., and Somorjai, G. A., *J. Chem. Soc. Faraday Trans. 1* **83,** 2061 (1987).
6. Badyal, J. P. S., Gellman, A. J., Judd, R. W., and Lambert, R. M., *Catalysis Letters* **1,** 41 (1988); and in preparation.
7. Thomas, G. E., and Weinberg, W. H., *J. Chem. Phys.* **70,** 1437 (1979).
8. Praline, G., Koel, B. E., Lee, H.-I., and White, J. M., *Appl. Surf. Sci.* **5,** 296 (1980).
9. Badyal, J. P. S., Gellman, A. J., and Lambert, R. M., *Surf. Sci.* **188,** 557 (1987).
10. Holland, L., Steckelmacher, W., and Yarwood, J., "Vacuum Manual," p. 52. E. and F. N. Spon Ltd., 1974.
11. Rhead, G. E., *J. Vac. Sci. Technol.* **13,** 603 (1976).
12. "Handbook of Chemistry and Physics," 68th ed., CRC Press. Boca Raton, FL, 1987–1988.
13. Schwarz, J. A., and Keleman, S. R., *Surf. Sci.* **87,** 510 (1979).
14. Madey, T. E., and Menzel, D., *Japan. J. Appl. Phys. Suppl.* **2,** 229 (1974).
15. Pfnur, H., and Menzel, D., *J. Chem. Phys.* **79,** 2400 (1983).
16. Hofmann, P., Gossler, J., Zartner, A., Glanz, M., and Menzel, D., *Surf. Sci.* **161,** 303 (1985).
17. Pfnur, P., Menzel, D., Hoffmann, F. M., Ortega, A., and Bradshaw, A. M., *Surf. Sci.* **93,** 431 (1980).
18. Thomas, G. E., and Weinberg, W. H., *J. Chem. Phys.* **70,** 1437 (1979).
19. Treichler, R., Riedl, W., Wurth, W., Feulner, P., and Menzel, D., *Phys. Rev. Lett.* **54,** 462 (1985).
20. Riedl, W., and Menzel, D., *Surf. Sci.* **163,** 39 (1985).

21. Yu, K. Y., Ling, D. T., and Spicer, W. E., *J. Catal.* **44,** 373 (1976).
22. Vickerman, J. C., Christmann, K., and Ertl, G., *J. Catal.* **71,** 171 (1981).
23. Shimizu, H., Christmann, K., and Ertl, G., *J. Catal.* **61,** 412 (1980).
24. Feulner, P., and Menzel, D., *Surf. Sci.* **154,** 465 (1985).
25. Yates, J. T., Jr., Peden, C. H. F., Houston, J. E., and Goodman, D. W., *Surf. Sci.* **160,** 37 (1985).
26. Peebles, D. E., Schreifels, J. A., and White, J. M., *Surf. Sci.* **116,** 117 (1982).
27. Doering, D. L., and Semancik, S., *Surf. Sci.* **175,** L730 (1986).
28. Blyholder, G., *J. Phys. Chem.* **68,** 2772 (1964).
29. Weimer, J. J., Umbach, E., and Menzel, D., *Surf. Sci.* **159,** 83 (1985).
30. Dry, M. E., Shingles, T., Boshoff, L. F., and Oosthuizen, G. F., *J. Catal.* **15,** 190 (1969).
31. Weimer, J. J., and Umbach, E., *Phys. Rev. B* **30,** 4863 (1984).
32. dePaola, R. A., Hrbek, J., and Hoffmann, F. M., *J. Chem. Phys.* **82,** 2484 (1985).
33. Fukuda, Y., Honda, F., and Rabalais, J. W., *Surf. Sci.* **91,** 165 (1980).
34. Hoffmann, F.M., Hrbek, J., and dePaola, R. A., *Chem. Phys. Lett.* **106,** 83 (1984).
35. Harrison, K., Prince, R. H., and Lambert, R. M., *Surface Sci.*, in press.
36. Sanz, J., Rojo, J. M., Malet, P., Munuera, G., Blasco, M. T., Conesa, J. C., and Soria, J., *J. Phys. Chem.* **89,** 5472 (1985).
37. Nix, R. M., Rayment, T., Lambert, R. M., Jennings, J. R., and Owen, G., *J. Catal.* **106,** 216 (1987).
38. Kikuchi, E., Matsumoto, M., Takahashi, T., Machino, A., and Morita, Y., *Appl. Catal.* **10,** 251 (1984).
39. Vannice, M. A., and Garten, R. L., *J. Catal.* **63,** 255 (1980).
40. McClory, M. M., and Gonzalez, R. D., *J. Catal.* **89,** 392 (1984).
41. Enomoto, T., Kata, K., Okuhara, T., and Misono, M., *Bull. Chem. Soc. Japan* **60,** 1237 (1987).
42. Yang, C.-H., and Goodwin, J. G., Jr., "Proceedings, 8th International Congress on Catalysis, Berlin, 1984," Vol. 5, p. 263. Dechema, Frankfurt-am-Main, 1984.
43. Chen, B. H., and White, J. M., *J. Phys. Chem.* **87,** 1327 (1983).